Journal of Colloid and Interface Science 587 (2021) 162–172

Contents lists available at ScienceDirect

Journal of Colloid and Interface Science

journal homepage: www.elsevier.com/locate/jcis

Regular Article

Moulding of micropatterned nanocellulose films and their application in fluid handling

Christine Browne, Gil Garnier, Warren Batchelor *

Bioresource Processing Research Institute of Australia, Department of Chemical Engineering, Monash University, Clayton, VIC 3800, Australia

GRAPHICAL ABSTRACT

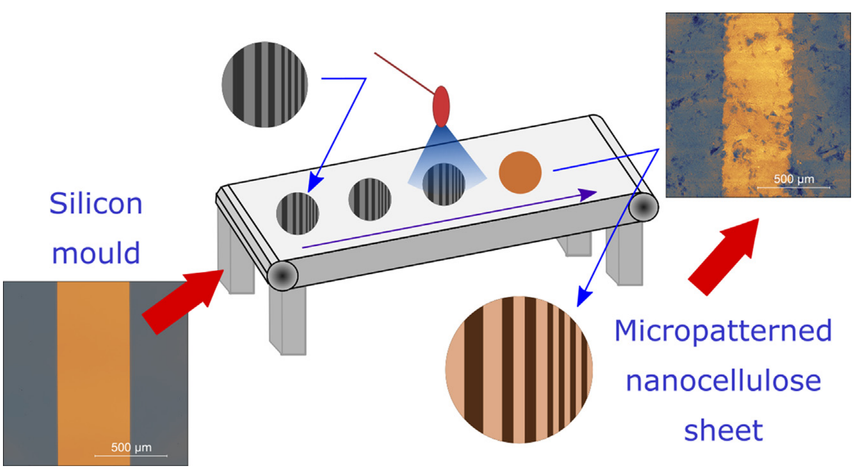

ARTICLE INFO

Article history:
Received 3 June 2020
Revised 29 November 2020
Accepted 30 November 2020
Available online 3 December 2020

Keywords:
Nanocellulose
Moulding
Micropattern
Spray coating
Photolithography
Deep reactive ion etch
Patterned roughness
Aspect ratio
Wicking

ABSTRACT

Hypothesis: Well-controlled micropatterned nanocellulose films are able to be fabricated via spray coating onto a micropatterned impermeable moulded surface. The micropattern size is able control the directionality of wicking fluid flow.

Experiments: Using photolithography and etching techniques, silicon moulds with channel widths of 5–500 μm and depths of 6, 12 and 18 μm were fabricated. Micropatterned nanocellulose sheets were formed by spray coating nanofibre suspensions onto the moulds. We also investigate the effect the dimensions of these micropatterned nanocellulose films have on wicking fluids.

Findings: Micropatterns were imparted on the surface of nanocellulose films which resulted in three well-defined regimes of conformation with the moulds: full, partial and no conformation. These regimes were driven by the aspect ratio (channel depth/width) of the moulds. Achieved channel widths and depths were compared to those possible with other micropattern fabrication techniques. The directionality of the wicking water droplets can be controlled with the micropatterned channel. Channels within the full conformation regime resulted in increased directionality of fluid flow compared with those not within this regime. This research demonstrates the industrially scalable process of spray coating has potential to serve as the foundation for a new generation of paper-based microfluidic devices.

Abbreviations: DRIE, deep reactive ion etch; PDMS, poly(dimethylsiloxane); SEM, scanning electron microscopy; AFM, atomic force microscopy.

* Corresponding author.

E-mail addresses: christine.browne@monash.edu (C. Browne), gil.garnier@monash.edu (G. Garnier), warren.batchelor@monash.edu (W. Batchelor).

https://doi.org/10.1016/j.jcis.2020.11.125
0021-9797/

1. Introduction

Cellulose is a natural polymer, which is biocompatible, biogradable and recyclable. It offers a suitable substitute for polymers derived from oil-based sources [1,2]. Nanocellulose materials, a subset of cellulose-based materials, contain fibres which have diameters within the nanometre scale which are typically less than 100 nm [1,3]. Nanocellulose fibres are liberated from cellulose materials through a series of mechanical, chemical or enzymatic treatment steps [1,4–6]. Due to their size these fibres offer many advantages that larger cellulose fibres do not, such as high strength, increased surface area, transparency, good biodegradability and renewability [1,3,7].

The current challenges with using cellulose-based products, when compared to plastic-based alternatives, is the ability to produce a high-quality surface finish and precise patterning of the material at the micrometre scale. These are important factors that need to be addressed to see increased usage of cellulose-based materials in applications such as microfluidics [8,9]. Various techniques such as laser cutting [10–13], wax printing [14–17] or even stamping [18,19] have been investigated to shape, pattern and fabricate cellulose-based products with the desired properties and features. The challenge with these techniques is the resolution or the size limitation of the features which are able to be formed. The use of laser cutting routinely creates features with clear definition at approximately 50 μm [10,12], with a recent study fabricating features of 24 μm [11] in dimension. Wax printing, whilst rapid, only fabricates one item at a time. The resolution is approximately 500 μm [14,15], with a recent study achieving 300 μm [16]. Another problem with this method is that it creates different surface properties in the printed and unprinted areas, which is undesirable for many applications. Stamping or embossing features is an alternative, though this process compacts, weakens and changes the arrangement of the fibres within the paper. Embossed structures with sizes down to 500 μm have been demonstrated [18,19].

The use of photolithography-based techniques allows the smaller features to be realised. Microprinting of gold features, which were formed with the use of photolithography and poly(dimethylsiloxane) (PDMS) stamping, onto cellulose-based films has been achieved down to size ranges of 6 μm [20,21]. Trimethlysilyl cellulose has been used as a photoresist to create patterns with a resolution of approximately 550 nm [22]. Whilst these techniques allow smaller feature sizes to be generated, they remove the ability to create depth into the surface.

Fluid wicking is the typical method for movement of fluids in paper-based microfluidic devices [23,24] including paper-based diagnostics [25–27]. For flow patterns emulating those achievable in glass or PDMS based devices, additional components in the cellulose matrix or a surface treatment process are required. Previously, it has been shown that the velocity of wicking fluid can be influenced by creating trenches within a wicking area of the paper-based microfluidic device [28]. Depending on the direction of these trenches, fluid flow was either accelerated (trenches in line with the flow) or retarded (trenches perpendicular to the fluid flow). This demonstrates that creating well defined micropatterns in cellulose-based materials offers great potential in fluid handling on microfluidic devices or potential for improvements in diagnostic applications.

In this study, we prepare micropatterned nanocellulose films. This is achieved through spray coating nanocellulose fibres onto the micropatterned moulds. These moulds are produced via photolithography and deep reactive ion etching (DRIE) which allows the production of well-defined channel widths and depths. This allows us to investigate the relationship between channel width and depth on the ability of the micropatterned nanocellulose films to conform to the mould. The effect of the micropatterns on water wicking is also examined to further understand the ability of these systems to be used in paper-based microfluidic devices. Due to use of nanocellulose fibres, the effect these fibre dimensions have on fluid flow is also investigated. As spray coating is an industrially scalable process, this work demonstrates a viable method to produce paper-based microfluidic devices at industrial relevant volumes.

2. Materials and methods

2.1. Materials

SU 8 2002 and SU 8 developer were sourced from Microchem. 2-propanol (> 99.5%) and sulfuric acid (> 95%) were received from Sigma Aldrich. The cellulose material (Celish KY-100S) was sourced and used as received from Daicel FineChem Industries. This material is also commonly known as micro-fibrillated cellulose (MFC) but in this study we will refer to it as nanocellulose. The supplied material had a concentration of 25 wt% with a putty like consistency. These fibres have an average diameter of 70 nm [29,30] with an aspect ratio of 123 [29]. Milli-Q water with a resistivity of 18.2 MΩ.cm was used. P-type doped silicon wafers with a diameter, thickness and orientation of 100 mm, 525 ± 25 μm and (100), respectively, were sourced from Electronics and Materials Corporation Limited. Queen blue food dye was used as received.

2.2. Methods

The main processing steps to create micropatterned nanocellulose sheets are shown in Fig. 1. This shows the main steps, which are the production of the moulds with the desired patterns and then the use of spray coating to form the micropatterned nanocellulose sheets.

2.2.1. Mould production

The moulds used within this study were fabricated into silicon wafers with photolithography and deep reactive ion etching (DRIE). These techniques allowed fine control of the resultant mould patterns.

The photomask was designed using KLayout (version 0.25.4) and the photomask was fabricated at the Minnesota Nano Center. This mask consisted of six regions where the channel widths were 500, 250, 100, 50, 10 and 5 μm.

The silicon wafers were then spun with SU 8 2002 photoresist on a spin coater (Laurell Technologies, WS-650-8B). The spin settings were 500 rpm for 10 s with an acceleration of 100 rpm/s and then 2000 rpm for 30 s with a 300 rpm/s acceleration. The wafer with applied photoresist, then underwent a soft bake for 2 min at 95 °C. A UV flood source (ABM-USA) provided an exposure energy of 100 mJ/cm^2 which was followed with a post exposure bake for 3 min at 95 °C. The design was then developed with the use of SU 8 developer for 1 min. The subsequent wafer was rinsed with 2-propanol and then dried under nitrogen.

The silicon wafer with the applied photoresist was then placed within the DRIE instrument (Oxford Instruments, PlasmaLab100 ICP380). The number of cycles were varied to obtain the required etch depths of 6, 12 and 18 μm. Typical etch rates were approximately 0.25 μm/cycle. The remaining SU 8 2002 was removed with sulfuric acid at 130 °C for 10 min. The wafer was then rinsed with Milli-Q water and dried under nitrogen. To remove any remaining photoresist the wafer was cleaned with a O_2 plasma for 10 min within the DRIE instrument.

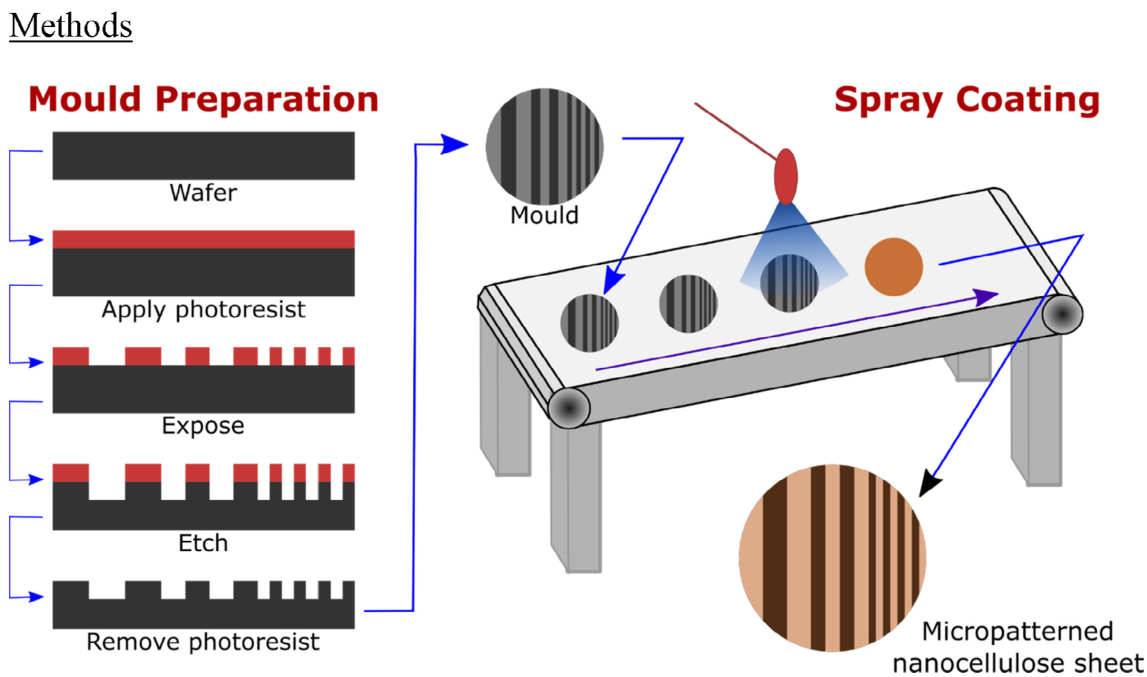

Fig. 1. Schematic diagram demonstrating the experimental process of producing micropatterned nanocellulose sheets.

2.2.2. Cleaning of silicon moulds prior to use

As the moulds were reused for each experiment, they were soaked in Milli-Q water to remove any remaining nanocellulose from previous experiments. The wafers were then further cleaned in a benchtop ultrasonic cleaner (Soniclean, 250HD) for 20 min in Milli-Q water. This liberated any remaining material trapped within the channels.

2.2.3. Production of patterned nanocellulose sheets

Never-dried nanocellulose fibres were mixed with distilled water to produce a 1.5 wt% nanocellulose fibre suspension. This suspension was then disintegrated for 15,000 revolutions (Messmer Instruments Limited, Disintegrator MK IIIC).

The sheets were produced with a rapid spray coating method developed by Shanmugam and co-workers [31,32], except that in this case the produced suspension was sprayed onto the silicon moulds. The suspension was sprayed onto the moulds with a spray coater (Wagner, ProjectPro 117 airless). The moulds were placed on a conveyer belt which was moving with a velocity of 2.4 cm/s underneath the spray nozzle. The nozzle tip (model 315) was located 45 cm above the conveyor belt and produced an oval shaped spray area. The moulds were passed under the spray nozzle three times and then placed overnight in a laboratory oven (Thermoline Scientific, model 01000F-440-D) at 50 °C to dry. Once the nanocellulose sheets were dry they were removed by carefully peeling the sheets off the moulds. With this method, the basis weight of the prepared nanocellulose sheets was approximately 80 g/m^2 and a thickness of 99 ± 8 μm.

2.2.4. Laser cut channels

Channels were cut with an Epilog Helix Laser Cutter at a power of 30 W, a speed of 63 mm/*sec* and a 2.0 lens module. This was conducted with a DPI of 1200 and a 2500 Hz frequency into paperboard (1000 gsm, Quill Paper, Australia). CorelDraw X5 was used to create channels with widths of 200 and 500 μm both parallel and perpendicular to the direction of travel by the laser. The channels created were then imaged with the optical profilometer.

2.2.5. Surface characterisation

The moulds, moulded patterns and laser cut channels were analysed using an OLS 5000 optical profilometer (Olympus Corporation). The data were analysed using the software supplied with the instrument (Analysis application, version 1.3.1.139) or Gwyddion (version 2.53).

2.2.6. Wicking of water droplets

A schematic diagram shown as Fig. 2 highlight the key steps in the wicking of water droplet measurements. Either 5 or 10 μL droplets were pipetted onto the samples to observe the wicking patterns. These droplets consisted of a 3 v/v% solution of blue food dye diluted in Milli-Q water. Previous work has shown that at these concentrations wicking of the fluid is not affected by the food dye, but the added contrast it provides reduces the noise within the measurements [33]. This process was completed at a room temperature of 23 °C and a relatively humidity of 50%. The droplets were allowed to completely dry and imaged with the use of a high-resolution scanner. The resultant fluid wicking patterns were analysed with ImageJ (1.52U). Care was taken to ensure the length of the wicked area was taken in parallel to the microchannels and the width taken across the direction of the channels. As the resultant analysis relied on the calculation of the elongation ratio of the wicked area, the data from the different sized droplets was able to be collated.

3. Results and discussion

The channel widths were 5, 10, 50, 100, 250 and 500 μm across all channel depths and along with the channel depths shown in Table 1. The channel depths were controlled by varying the number of cycles the wafer was subjected to during the DRIE processing step and the depths were 6, 12 and 18 μm. The channels were characterised by their aspect ratio defined as depth divided by width of the channels (Table 1). The aspect ratio varies from 3.6 for the 5 μm wide channel with an 18 μm depth to 0.012 for the 500 μm width and 6 μm depth channels.

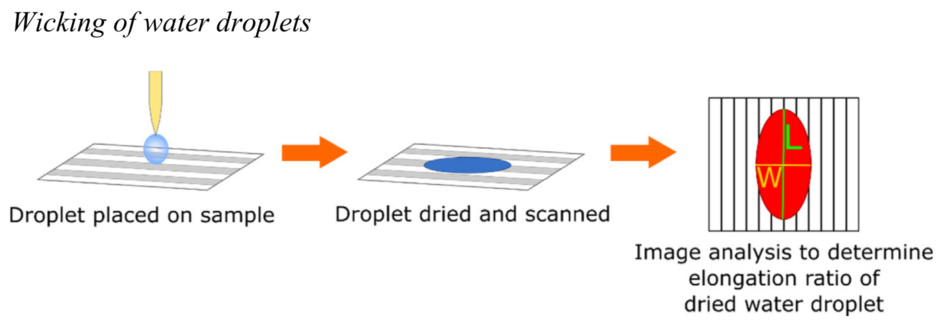

Fig. 2. Schematic diagram highlighting the main steps in the wicking of water droplet measurements. Where the elongation ratio is defined as length (L) divided by width (W) of the wicked area.

Table 1
List of the various channel widths and depths used with their aspect ratios (depth/width).

Channel width (μm)	Depth (μm)		
	6	12	18
5	1.2	2.4	3.6
10	0.6	1.2	1.8
50	0.12	0.24	0.36
100	0.06	0.12	0.18
250	0.024	0.048	0.072
500	0.012	0.024	0.036

The selection of photolithography and DRIE to produce the moulds allowed channels of resolution as high as 5 μm wide and 6 μm deep to be formed. Techniques such as 3D printing and laser cutting have only recently produced resolutions of 20 μm [34] and 24 μm [11], respectively. Whilst some of the dimensions used within this study could have been produced with 3D printing or laser cutting, the use of photolithography and DRIE allowed the moulds for all samples to be manufactured from the same material. This limits any variations due to changes in surface interactions between the fibre suspension and the mould.

3.1. Imaging and analysis of samples

The nanocellulose sheets produced are analysed by optical profilometery and Fig. 3 demonstrates the typical images. Fig. 3a) shows a typical image of the silicon mould with a channel width of 500 μm and depth of 6 μm. The height profile of this image (Fig. 3c) shows the expected channel depth and width. It is also important to note the sharp and distinct change in height which occurs within the mould. This occurs across all channel widths and depths and allows us to make comparison across different moulds without considering the gradient of the wall.

Fig. 3b) shows the resultant moulded nanocellulose sheet and the height profile for this sample is shown as Fig. 3d). These images demonstrate that micropatterned channels can be clearly reproduced at these dimensions. This imaging was completed for all samples and the resultant channel widths and depths were measured to determine the extent of fidelity between the moulds and nanocellulose sheets.

Optical profilometry offers many advantages for imaging these samples over other techniques such as scanning electron microscopy (SEM) and atomic force microscopy (AFM). Optical profilometry is able to gain the height profile or surface topography over areas larger than 120 × 120 μm, whereas this is typically the maximum dimension achievable with AFM. The image resolution and quality of SEM are also better than optical profilometry but are constrained by the image size. A large SEM image might cover a single channel which is insufficient to characterise the quality of the surface; SEM also lacks the height data.

Comparing the images of the silicon mould (Fig. 3a)) with those of the micropatterned nanocellulose film (Fig. 3b)) reveals small imperfections within the nanocellulose film. These small imperfections are present in every paper sample. This is due to many factors such as the distribution or arrangement of the fibres in the resultant film and entrained air bubbles in the suspension. A previous study demonstrated that forming nanocellulose films onto silicon wafer base substrates resulted in a lower root mean square (RMS) roughness, or a lower level of imperfections, than other substrates [35].

This study identified three different regimes of conformation or fidelity between the mould and resultant samples with examples shown in Fig. 4. The three regimes are: full conformation (Figs. 3b and 4a), partial conformation (Fig. 4b)) and no conformation (Fig. 4c)). For ease of comparison, each average height profile shown in Fig. 4 was determined by calculating the mean height in each vertical pixel line.

Full conformation is a region where the micropatterns on the surface of the nanocellulose sheet have a high fidelity with the mould as demonstrated by the schematic diagram in Fig. 4a). In cases of full conformation, both the width and depth of the channel in the sheet were matched with that of the mould. The optical profilometry image and the average height profile also show that the 250 μm wide and 6 μm deep channel is well-defined on the surface of the nanocellulose sheet.

Partial conformation occurs when either the width or depth, individually or simultaneously, of the pattern does not fully replicate the mould. It can be seen that the left most high ridge of the channel in Fig. 4b) demonstrates good conformation with regards to channel width though the depth does not reach the expected 12 μm. In the other two high sections of the channels both the width and depth do not show good fidelity with the mould.

No conformation is when there is no evidence of micropatterning in the surface of the produced nanocellulose sheets. The example shown in Fig. 4c) is for 5 μm wide and 12 μm deep channels and clearly shows no evidence of micropatterning on the surface of the sheet, with only random variation of the roughness across the x-axis. In this optical profilometry image the network of nanocellulose fibres are visible and any height changes in this regime is due to the inherent surface roughness of the formed nanocellulose sheet.

3.2. Micropatterned nanocellulose sheets

From the optical profilometry imaging, the aspect ratio of the resultant channels within the micropatterned nanocellulose films were determined. An example of these images is shown in the supporting information (Fig. S1). These values were then plotted

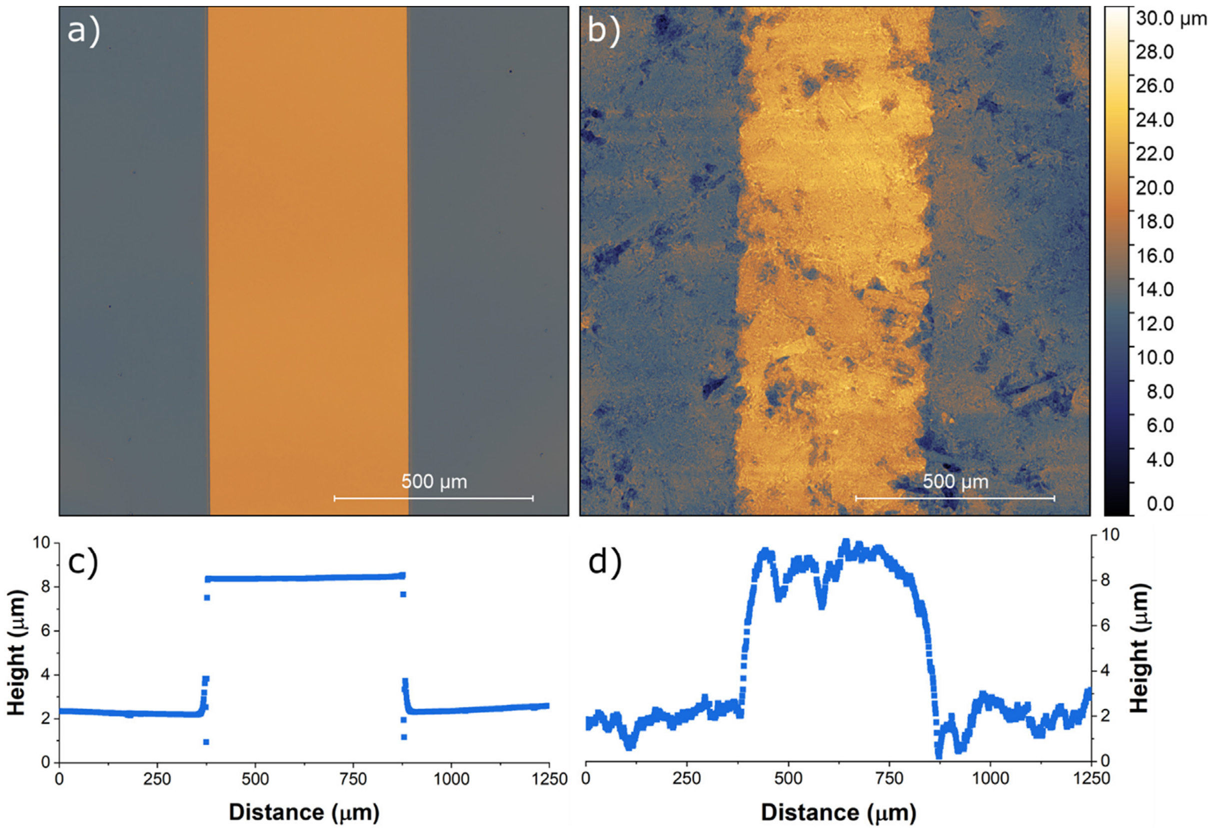

Fig. 3. Typical optical profilometry images. The images shown here are for a 500 μm width and 6 μm depth channel. a) Image of the prepared silicon mould. b) Image of the resultant nanocellulose film. c) Typical height profile of the prepared silicon mould. d) Typical height profile of the resultant patterned nanocellulose film. The minimum height of the profiles was set to 0 for ease of comparison.

against the aspect ratio of the mould to generate Fig. 5. Aspect ratio is defined as depth/width. A spline fit (dashed purple line) was applied to the data and demonstrates the relationship between the aspect ratio of the mould and sample. When the mould aspect ratio values were greater than 0.7 all have a sample aspect ratio of 0, or no conformation, and were not shown in Fig. 5 for increased clarity. These data are shown in the supporting information (Fig. S2). The data plotted in Fig. 4 were separated into the three different mould depths studied. The dotted line is a 1:1 line which demonstrates where the aspect ratio between the mould and the sample are identical, indicating a region of full conformation. The points with the lowest mould aspect ratios (up to values of approximately 0.1) match the 1:1 line very well and indicate a regime of full conformation. The lowest aspect ratios correspond to the channel width of 500, 250 μm and 100 μm (with a 6 μm mould depth) and this demonstrates that the larger the channel width, the easier it is to mould (full conformation). These values are similar to those achievable with wax printing [14–16] and embossing [18,19] but with the added benefit of the paper properties remaining the same for all three walls within the channel.

From a mould aspect ratio ranging from 0.1 to 0.5, significant deviation from the 1:1 line is observed, indicating full conformation no longer occurs. Firstly, there is a slight increase in the sample aspect ratio when compared to that of the mould (at approximately 0.12). In this region, there is a slight decrease in the conformation in the channel depths. Typically, there are regions of the resultant sheet that have complete fidelity with respect to the depth of the mould and some regions where the expected channel depth has decreased slightly (Fig. 4b). This observation explains the increase in the error bar values associated with the partial conformation region when compared to that of the full conformation region. When the mould aspect ratio increases further to values of 0.2 to 0.5, the sample aspect ratio decreases significantly compared to the mould. In this range, both the channel widths and depths of the mould no longer have a high fidelity with the sample. Due to the reduced fidelity with the mould, the variation in the measured widths and depths greatly increases, hence the increase in the error bars in this region. These mould aspect ratios correspond to that of the 50 and 100 μm wide channels with depths of 12 and 18 μm, which are similar to previously reported values achieved via laser cutting [10–12].

Once the mould aspect ratio was greater than 0.5, the no conformation region was reached. An aspect ratio of 0.5 and greater corresponds to channel widths of 5 and 10 μm at all depths investigated. This indicates that a 1.5 wt% suspension of nanocellulose fibres used here is not suitable to form micropattern channels of 10 μm and lower in value.

The full and partial conformation regimes are examples where for a set channel width, variations in depth cause the conformation regime to change. The 100 μm wide channel with a depth of 6 μm is within the full conformation regime; all other depths investigated belong to the partial conformation regime. Another example is the two data points at a mould aspect ratio of 0.12; both provide the same sample aspect ratio of 0.15. These two points correspond to channel widths of both 50 and 100 μm with different mould channel depth. These examples demonstrate that mould aspect ratio plays a critical role in determining the conformability of the suspension the mould.

The use of high resolution optical profilometry with both the height and laser intensity channel show the fibre orientation within a 250 μm wide and 12 μm deep channel are shown as Fig. 6. This channel is within the full conformation regime as

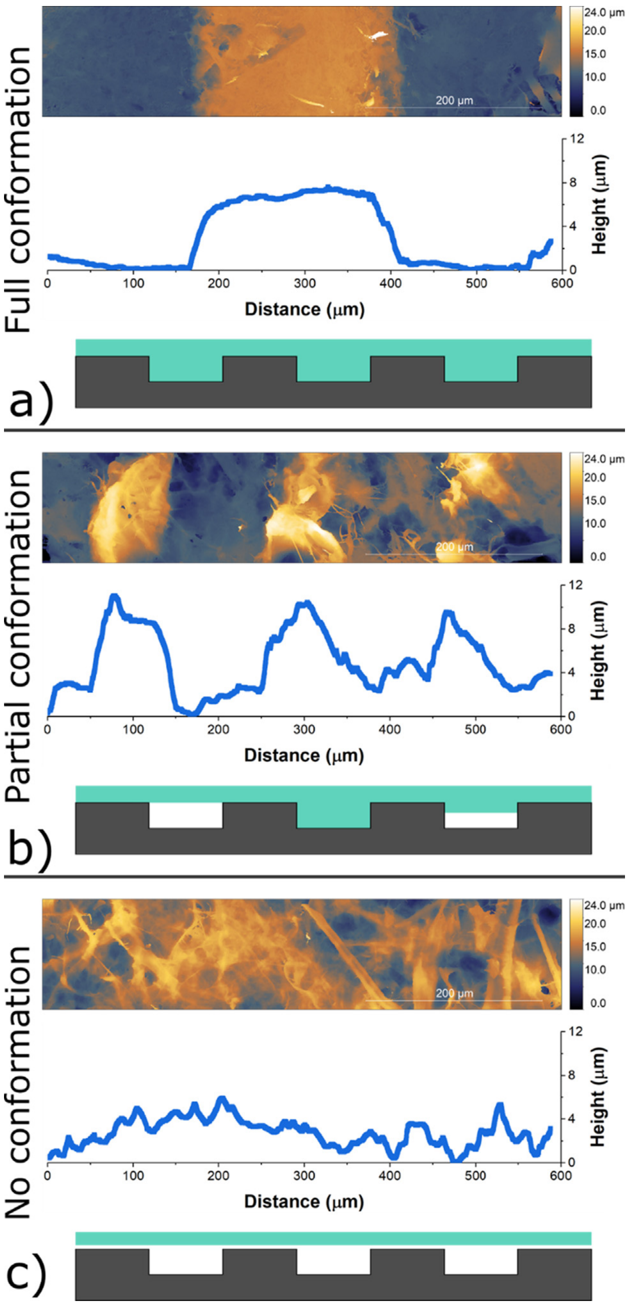

Fig. 4. Optical profilometry images, averaged height profiles and schematic diagrams (top to bottom in each section) of the three different conformation regimes: a) full conformation (mould channel width of 250 μm and 6 μm depth). b) partial conformation (mould channel width of 100 μm and 12 μm depth). c) no conformation (mould channel width of 5 μm and 12 μm depth). The minimum height of the profiles was set to 0 for ease of comparison.

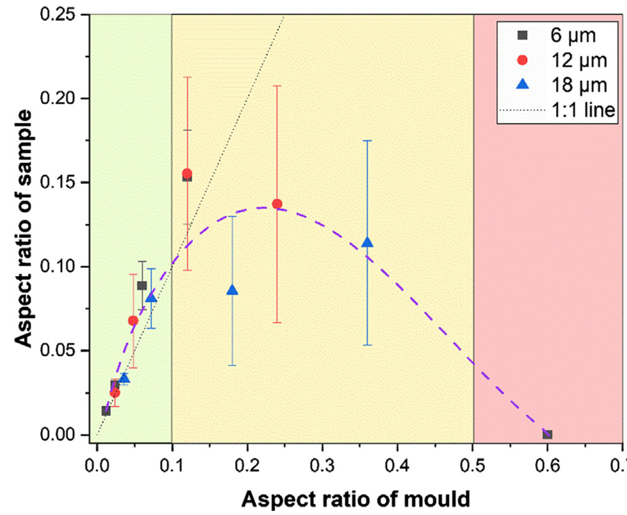

Fig. 5. Aspect ratio of mould versus the measured aspect ratio of the 1.5 wt% micropatterned nanocellulose sheets. The data shown is for 6 μm (black squares), 12 μm (red circles) and 18 μm (blue triangles) mould depths. A 1:1 line was plotted to indicate the area where the mould and sample dimension match. The dashed purple line is the spline fit for all of the nanocellulose data. The shaded areas correspond to the different conformation regimes which are from left to right full conformation (green), partial conformation (yellow) and no conformation (red). (For interpretation of the references to colour in this figure legend, the reader is referred to the web version of this article.)

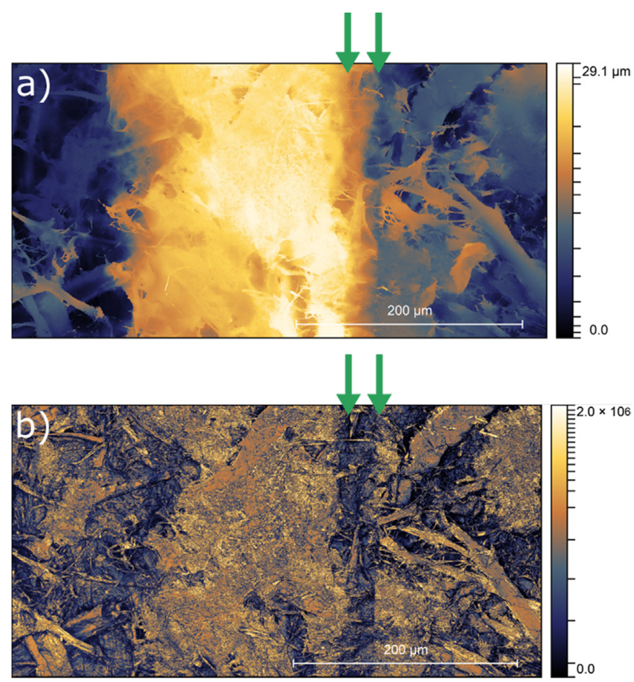

Fig. 6. High resolution optical profilometry images of channels with a width of 250 μm and a depth of 12 μm. (a) Height channel image. (b) Laser intensity channel image.

shown by the height channel image (Fig. 6a)). The image of Fig. 6b) is of the laser intensity channel and highlights the location of the fibres within the sheets and demonstrates the minimal effect the sidewalls of the mould have on the resultant ability of the fibres to conform.

The first step of a DRIE process is the etch cycle, where the silicon is etched with a plasma and is followed by a passivation cycle where C_4F_8 molecules coat the walls and bottom of the etched silicon wafer [36]. The C_4F_8 molecules at the bottom of the channel are fully removed during the following plasma etch step whilst the molecules on the walls are not. This protects the walls from further etching in the following etch steps but does cause scalloping of the sidewalls [37]. This, in turn, increases the surface roughness of the channel sidewalls when compared to the top and bottom of the channels. As all channels were fabricated with the same method, it is reasonable to assume that the channel sidewalls surface roughness is similar for all moulds.

Even though the sidewalls have an increased surface roughness from the DRIE processing, the influence of this would be minimal in this system. This is demonstrated in Figs. 3 and 6 for full conformation regime samples. When the height profiles of the mould (Fig. 3c)) and the sample (Fig. 3d)) are compared, the change in height between the high and low parts of the channel in the mould are nearly vertical or occurs over a very small distance (eg. on the order of nanometres). The transition distance from the bottom to the top of the channel is on the order of micrometres and the gradient of this section is visibly lower in the sample. Fig. 6 also demonstrates the sample not contacting the sidewalls which is highlighted with laser intensity images. The green arrows on Fig. 6b) indicate the region where the nanocellulose fibres are not in contact with the silicon surface of the top or bottom of the channel. This is a distance of 30 μm which is difficult to see on the height image (Fig. 6a)) of the same region. This analysis indicates that due to bending and the flexibility of the fibres in the suspension, the fibres are less likely to come in full contact with the sidewalls; therefore, the increased surface roughness of this area does not influence conformation of the samples.

The optical profilometer images (Fig. 6) demonstrate that fibres do not have any specific orientation in the channels or the films. The moulds are sprayed in their normal direction and the suspension is then dried, forming a network of random fibres orientation.

3.3. Shape profiles of laser cut channels

The shape profile of channels produced via laser cutting is shown in Fig. 7. Laser cut channels with widths of 200 and 500 μm were produced and imaged by optical profilometry to measure the height profiles. The features created in the parallel and perpendicular direction of laser travel were investigated.

Channels designed to have widths of 500 μm had depths of approximately 300 μm in both the perpendicular and parallel laser travel directions. The channel widths were approximately 560 μm and 650 μm for the parallel and perpendicular directions, respectively. For the 200 μm wide channels those made with the laser in the parallel direction are 320 and 270 μm, wide and deep, respectively; those made from the perpendicular laser travel are 340 and 150 μm, respectively. For 200 μm wide channels, discrepancy between the laser travel directions is measured both in width and depths and this is due to the operation of the laser. The laser is programmed to either be on or off, either etching or not. This explains the greater accuracy to the design values when the laser is travelling in the parallel direction as the laser has a longer transition time between the on/off states. In the perpendicular direction, this time frame is dramatically shorter which decreases the accuracy. The parallel direction results in increased depth for the 200 μm width channels due to this on/off transition time; however, when width is increased to 500 μm, the changes in depth are no longer measurable.

The shape of the resultant channels also varies based on the channel widths. The 500 μm wide channels have a more rounded shape at the bottom, whereas the 200 μm wide channels have a v-shaped profile. This change in shape is also due to the laser operation. Another advantage of the moulding technique is presented by comparing the channel shape of the full conformation regime profiles (Figs. 3d and 4a). As the nanofibres are sprayed in the normal direction to the mould surface, there are no changes in the channel profile due to directionality. Using laser cutting, the channel dimensions and shape vary with the direction of laser travel. This would drastically affect the operation of microfluidic devices where regular flow and often laminar flow are required.

3.4. Moulding performance compared to other techniques

A comparison of the possible width verses depth of channels created within paper material using various techniques is presented in Fig. 8. The techniques compared here are wax printing, microembossing, laser cutting and the results from this study for moulding. Typically, wax printing and microembossing are unable to fabricate channels narrower than 300 μm [14–16,18]. The possible channel depths with these techniques are also limited. Wax printing applies a hydrophobic wax to create hydrophilic areas where fluid is able to wick, which means no depth is possible at all within this technique. A minimum depth of 50 μm is possible using microembossing as fluid wicking is controlled by applying pressure to both sides of the material which compacts the fibres to create regions of low and high porosity [18]; thickness of the paper material is thus important. The thickness of the paper used for microembossing ranged between 180 and 390 μm; it is considerably larger than the thickness of the micropatterned nanocellulose films which are 99 ± 8 μm thick. The application of heat during embossing has allowed higher resolutions to be achieved with thermoplastic materials [38]. The lack of water content within cellulose-based films means the fibres are fixed in place within the fibre network and would not result in an increase in resolution. These constraints mean channels of lower depths are difficult to create by microembossing.

Typically, laser cut channels are made by complete breakthrough of the paper source and a backing material such as foil or plastic is laminated on to the back surface of the paper [39]. Due to paper breakthrough, studies in this area typically focus on improvement in the resolution of channel width and do not focus on the channel depth as this is controlled by the paper thickness. Currently, the best resolution considering both channel width and depth has been a 55 μm wide channel within a regenerated cellulose material (point 1 in Fig. 8). A channel width of 24 μm was demonstrated in a nitrocellulose material but the depth increased to 135 μm [11]. When more typical cellulose fibres are considered, the channel width resolution decreased to 103 μm and was shown to be limited by the fibre diameter, eg. smaller fibres equate to smaller channel widths [11]. Other studies have generated channels without breaking through the paper source [10,12,13]. Channel widths of 62 μm and 50 μm depth were possible in a silicon coated parchment paper where the laser cutter changed the hydrophobic areas of the coating into hydrophilic areas [12]. Channel widths and depths of 150 and 135 μm, respectively, were possible in a nitrocellulose material with breakthrough of the paper [10]. This study demonstrated channels which were able to wick fluids along them without breakthrough but did not provide a measurement of the achievable channel depths. The material of paperboard has also demonstrated channel depths of 85 μm and widths of 500 μm were possible and investigating further width and depth combinations was not the focus of the study [13].

We have demonstrated in Fig. 8 that the moulding technique is able to generate channels with a minimum width of 50 μm up to 500 μm. The possible depths at lower channel widths were 5 and 9 μm for the 50 and 100 μm channel width channels, respectively. Depths up to 18 μm were possible once the channel width was increased to 250 μm. Unlike the other methods, the depth is constrained by the interaction of the fibres within the suspension and the dimensions of the mould making wider and shallower channels easiest to fabricate. Other techniques require removal or compaction of material to create the channels making deeper channels easier to fabricate. It is envisioned that with changes to the moulds that wider and deeper channels would be possible to fabricate as indicated by the region indicating the proposed dimension achievable with moulding in Fig. 8. This region was determined by considering the achievable mould aspect ratios of the full conformation regime up to a channel width of 500 μm, where the aspect ratio of 0.1 equates to a channel depth of 50 μm. As the average thickness of the nanocellulose film was 99 ± 8 μm, the proposed depth at channel widths larger than 500 μm were not

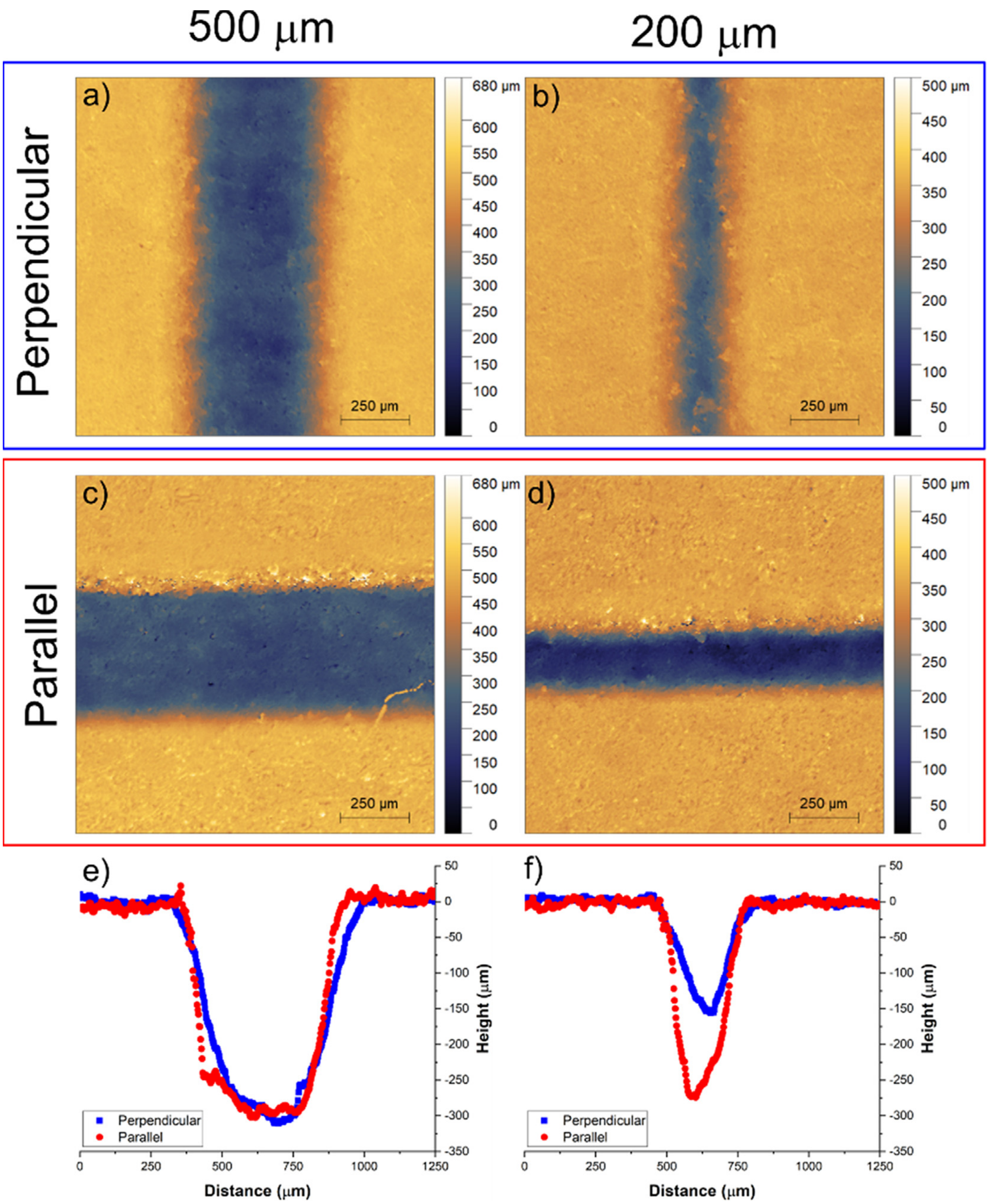

Fig. 7. Optical profilometry and height profiles of laser cut channel with channel widths of 200 and 500 μm. Images of channels produced in the perpendicular direction of laser travel a) 500 μm, b) 200 μm. Images of channels produced in the parallel direction of laser travel c) 500 μm, d) 200 μm. Height profiles of the channels produced e) 500 μm, f) 200 μm. The maximum height of the profiles was set to 0 for ease of comparison.

increased as it would be difficult to maintain the structure of the channels at larger channel depths. The moulding technique allows channel dimensions previously unattainable within cellulose-based materials and opens the possibility of further miniaturisation of paper-based microfluidic devices.

3.5. Wicking of water droplets

The effect of the micropatterned channels and the region of conformation, full or partial conformation, on fluid flow were studied with dyed water droplets. The droplets were allowed to fully dry before extracting the elongation ratio of the wicked water droplet area left by the dye. The elongation ratio of the 5 and 10 μL drops were similar and were therefore combined in this study. The mould channel width and these elongation ratio values are shown in Fig. 9. As the channel width increases and moves from a region of partial to full conformation for all channel depths, the elongation ratio of the droplet also increased. This indicates that the presence of micropatterned channels and the extent of channel conformation directs fluid flow during the wicking process. It also highlights the possibility of micropatterned nanocellulose films for paper-based microfluidics.

The elongation ratio for a water droplet placed on a smooth nanocellulose surface (eg. no channels on surface) was 1.03 ± 0.10. This elongation ratio increases to approximately 1.15 with the 50 and 100 μm channel width nanocellulose micropattern sheets. Both of these channel widths, except for the 100 μm wide and 6 μm deep channel, are located within the partial conformation regime for all depths. This indicates that the presence of channels of decreased fidelity do show a small increase in the

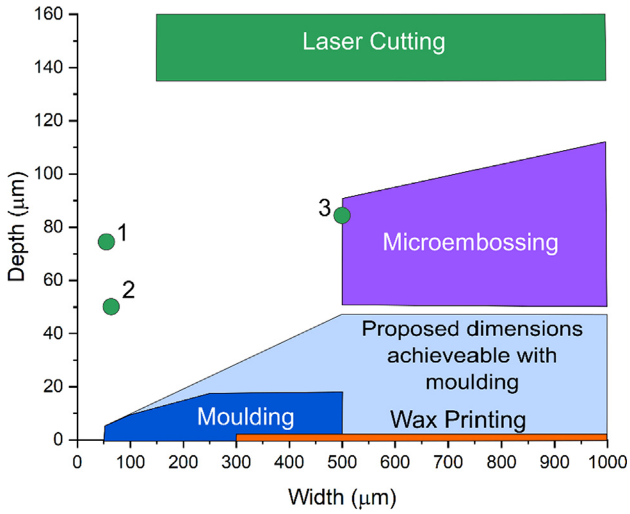

Fig. 8. Comparison of resolution of channel dimension for the techniques of moulding (dark blue), wax printing (orange) [14,15,17], microembossing (purple) [18] and laser cutting (green) [10]. Additional studies using laser cutting have been presented as the green points of 1 [11], 2 [12] and 3 [13]. Based on the achievable aspect ratios, the proposed channel depths and widths achievable with the moulding technique are shown in light blue. (For interpretation of the references to colour in this figure legend, the reader is referred to the web version of this article.)

directionality of the wicking fluid; this is significant for blood typing applications [26,33].

Once the channel width was increased to 250 μm, the elongation ratio of the resultant wicking pattern increased to approximately 1.2–1.3 for all channel depths. At this channel width, some separation of the elongation ratios is starting to occur with respect to the depth of the channel, though this is minimal at the 95% confidence interval. With the 6 μm channel depth demonstrating the lowest elongation ratio of wicking pattern and the 18 μm demonstrating the highest. This indicates an increase in the ability of the micropatterns to impart directionality on wicking fluids when fidelity with the mould is increased.

The same observations were made for the 500 μm channels as for the 250 μm channel, except the elongation ratio increased to approximately 1.3–1.4. Once again, the separation with respect to the channel depth is preserved with the 18 μm depth possessing the highest elongation ratio and the 6 μm the lowest, though this separation is minimal within the 95% confidence interval. This demonstrates that once channels are located within the full conformation regime feature sizes of at least 6 μm, the changes in channel depths, control the elongation ratio and fluid transport.

The size properties of nanocellulose fibres are desired over those of conventional wood fibres in this study. Conventional wood fibres, those used within standard pulp and packaging process plants, typically have diameters of 10–15 μm and lengths of 1 mm [7]. The diameters of the conventional wood fibres are larger than some of the feature sizes in the micropattern nanocellulose channels. This study demonstrates that fluid transport occurs on scale less than the diameter of the conventional wood fibres and even though these fibres offer large cost and energy benefits, would not be suitable to achieve the resolution and dimension of the micropatterned nanocellulose channels.

A previous study showed that an increase in channel width (depth was fixed in this particular study) decreased the 'mobility factor' [40]. The mobility factor is determined experimentally and incorporates the channel dimensions, viscosity and surface tension of the fluid. When this parameter becomes negative, this indicates that filling of the microchannels is no longer possible. Our observations of preferential wicking in the channel direction are contrary to this, but this previous study was completed in pyrex glass channels and does not have the added complication of wicking through the channel structure itself.

The wicking properties of cellulose-based materials have been studied extensively in the literature [14,27,28,33,41,42] and we are able to link our observations with previous studies. Previously, wax printing was used to create an area where water was able to wick through a chromatography paper over a set distance [28]. To emulate open microfluidic channels razor cut channels were

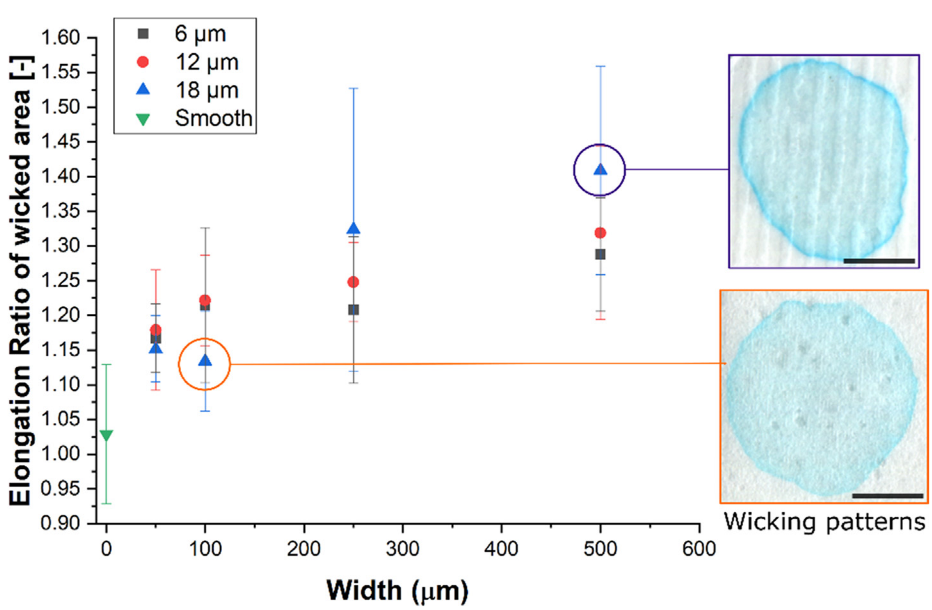

Fig. 9. Elongation ratio of the water droplet wicked area as extracted by image analysis and plotted against the mould channel width. Where channel depths of 6 μm (black squares), 12 μm (red circles), 18 μm (blue triangles) and the smooth surface (green upside-down triangles) are used. The error bars indicate the 95% confidence interval of the data. Images on the right are examples of the wicked area on the micropatterned nanocellulose sheets received from these experiments. The black scale bars indicate a distance of 3 mm. (For interpretation of the references to colour in this figure legend, the reader is referred to the web version of this article.)

created, which were parallel to the direction of fluid flow within the wicking area. Longer channels or increased area of paper removal resulted in larger decreases in the wicking time over the set distance [28]. This indicates that water will follow the channels preferentially over wicking through the fibrous cellulose material. This is similar to the observations of this study, where the widest and deepest channels provide the largest increase in elongation ratio of the wicked area.

The razor cut study also created channels in a perpendicular direction to fluid flow which caused an increase in the wicking time or retarded the flow to the same set distance [28]. This demonstrates that water prefers to flow along channels as opposed to the cross-channel or perpendicular direction. This would indicate that if micropatterned channels with sufficient depth were reached, the fluid flow during wicking could be limited to the direction of the channels and lead to increases in the measured elongation ratio. We also have the added complexity of the variation of conformation, or definition of the microchannels. In our case, we presume that our experimental observation of decreased elongation ratio within the partial conformation regime is due to it not offering the benefits of allowing water to travel in the microchannels without being subjected to wicking through the nanocellulose materials when compared to the full conformation regime.

The processing steps of disintegration and spray coating are unit operations all currently used at industrial scales. These can easily be adapted to create industrial volumes of micropatterned nanocellulose sheets. Spray coating allows large areas of micropatterns to be created quickly and the moulds are easily cleaned and fully reusable. Our process does not use organic solvents which minimises costs and lowers health and safety concerns. These aspects, along with the ability to predict the conformation regime, are important for the design and implementation of this process at industrial scales.

4. Conclusion

In this study, we demonstrated that fabricating micropatterned nanocellulose films with a minimum feature size of 50 μm is possible and these micropatterns also influence the fluid flow during the wicking process. This new and scalable process can precisely pattern nanocellulose fibres at the micrometre scale. This is comparable to values achieved with laser cutting [10,12] and exceeds the resolution achieved by either wax printing [16] (300 μm) or embossing [18,19] (500 μm). These other techniques are also unable to access the shallow channel depths which are possible with moulding. The precise patterning was accomplished by spray coating a suspension of nanocellulose fibres onto a silicon wafer with simple channel designs with micrometre widths. With the feature sizes achieved and the advantage of all three channel walls having the same surface and fibre network properties (unlike other currently used methods), micropatterned channels are a promising platform technology for the development of paper-based microfluidic systems.

The channel dimensions investigated ranged from 5 to 500 μm in width and differing depths of 6, 12 and 18 μm. These dimensions allowed the effect of aspect ratio (depth/width) of the mould to be investigated. We discovered three distinct conformation regimes governed by the aspect ratio. These regimes were full conformation where the depth and width of the channels was well replicated, partial conformation where either the depth and/or width no longer had high fidelity with the mould and no conformation where no micropatterns were imparted on the nanocellulose film.

The wicking of water droplets also demonstrated that the presence of microchannels increased the elongation ratio (length/width of wicked area) of the wicking droplet pattern. This ratio increased with both increasing channel width and depth of the micropatterns, demonstrating increased directionality during the fluid wicking process. These observations demonstrate the importance of the conformation regime on the fluid flow process with those channels located within the full conformation regime giving the higher elongation ratios. These results demonstrate great potential for applications in paper-based diagnostic tests. Further studies will be required to understand the interactions between blood components such as red blood cells, plasma and proteins with nanocellulose fibres and the micropatterns.

As the conformation of the micropatterns is driven by the aspect ratio of the mould, the resultant patterning can be tuned for a desired application. In the future, this could be extended to use nanocomposites such as carboxymethyl cellulose [35] to make the micropatterns. Micropatterned nanocellulose films offer many advantages in the area of paper-based microfluidics and this work demonstrates nanocellulose-based sources as an attractive alternative for further miniaturisation.

CRediT authorship contribution statement

Christine Browne: Conceptualization, Methodology, Formal analysis, Investigation, Writing - original draft, Writing - review & editing, Visualization. **Gil Garnier:** Conceptualization, Writing - review & editing, Supervision, Funding acquisition. **Warren Batchelor:** Conceptualization, Methodology, Writing - review & editing, Supervision, Project administration, Funding acquisition.

Reference Data

Data available in DOI: https://doi.org/10.26180/c.5230922.

Declaration of Competing Interest

The authors declare that they have no known competing financial interests or personal relationships that could have appeared to influence the work reported in this paper.

Acknowledgements

Funding from the Australian Research Council-Industry Transformation Research Hub; Processing Advanced Lignocellulosics (PALS) [Grant Number IH170100020] is gratefully acknowledged. This work was performed in part at the Melbourne Centre for Nanofabrication (MCN) in the Victorian Node of the Australian National Fabrication Facility (ANFF). Portions of this work were conducted in the Minnesota Nano Center, which is supported by the National Science Foundation through the National Nano Coordinated Infrastructure Network, Award Number NNCI-1542202.

Appendix A. Supplementary material

Supplementary data to this article can be found online at https://doi.org/10.1016/j.jcis.2020.11.125.

References

[1] N. Lavoine, I. Desloges, A. Dufresne, J. Bras, Microfibrillated cellulose – Its barrier properties and applications in cellulosic materials: A review, Carbohydr. Polym. 90 (2) (2012) 735–764.
[2] P. Phanthong, P. Reubroycharoen, X. Hao, G. Xu, A. Abudula, G. Guan, Nanocellulose: Extraction and application, Carbon Resour. Conversion 1 (1) (2018) 32–43.
[3] I. Siró, D. Plackett, Microfibrillated cellulose and new nanocomposite materials: a review, Cellulose 17 (3) (2010) 459–494.

[4] D. Klemm, B. Heublein, H.P. Fink, A. Bohn, Cellulose: fascinating biopolymer and sustainable raw material, Angew. Chem. Int. Ed. 44 (22) (2005) 3358–3393.
[5] S.J. Eichhorn, A. Dufresne, M. Aranguren, N.E. Marcovich, J.R. Capadona, S.J. Rowan, C. Weder, W. Thielemans, M. Roman, S. Renneckar, W. Gindl, S. Veigel, J. Keckes, H. Yano, K. Abe, M. Nogi, A.N. Nakagaito, A. Mangalam, J. Simonsen, A. S. Benight, A. Bismarck, L.A. Berglund, T. Peijs, Review: current international research into cellulose nanofibres and nanocomposites, J. Mater. Sci. 45 (1) (2010) 1–33.
[6] J. Hu, D. Tian, S. Renneckar, J.N. Saddler, Enzyme mediated nanofibrillation of cellulose by the synergistic actions of an endoglucanase, lytic polysaccharide monooxygenase (LPMO) and xylanase, Sci. Rep. 8 (1) (2018) 3195.
[7] S. Ang, V. Haritos, W. Batchelor, Effect of refining and homogenization on nanocellulose fiber development, sheet strength and energy consumption, Cellulose 26 (8) (2019) 4767–4786.
[8] T. Akyazi, L. Basabe-Desmonts, F. Benito-Lopez, Review on microfluidic paper-based analytical devices towards commercialisation, Anal. Chim. Acta 1001 (2018) 1–17.
[9] D.D. Liana, B. Raguse, J.J. Gooding, E. Chow, Recent advances in paper-based sensors, Sensors 12 (9) (2012) 11505–11526.
[10] P. Spicar-Mihalic, B. Toley, J. Houghtaling, T. Liang, P. Yager, E. Fu, CO_2 laser cutting and ablative etching for the fabrication of paper-based devices, J. Micromech. Microeng. 23 (6) (2013) 067003.
[11] M.A. Mahmud, E.J.M. Blondeel, M. Kaddoura, B.D. MacDonald, Features in microfluidic paper-based devices made by laser cutting: how small can they be?, Micromachines 9 (5) (2018) 220.
[12] G. Chitnis, Z. Ding, C.-L. Chang, C.A. Savran, B. Ziaie, Laser-treated hydrophobic paper: an inexpensive microfluidic platform, Lab Chip 11 (6) (2011) 1161–1165.
[13] M. Naseri, G.P. Simon, W. Batchelor, Development of a paper-based microfluidic system for a continuous high-flow-rate fluid manipulation, Anal. Chem. 92 (10) (2020) 7307–7316.
[14] E. Carrilho, A.W. Martinez, G.M. Whitesides, Understanding wax printing: a simple micropatterning process for paper-based microfluidics, Anal. Chem. 81 (16) (2009) 7091–7095.
[15] W. Dungchai, O. Chailapakul, C.S. Henry, A low-cost, simple, and rapid fabrication method for paper-based microfluidics using wax screen-printing, Analyst 136 (1) (2011) 77–82.
[16] E.B. Strong, S.A. Schultz, A.W. Martinez, N.W. Martinez, Fabrication of miniaturized paper-based microfluidic devices (MicroPADs), Sci. Rep. 9 (1) (2019) 7.
[17] K. Tenda, R. Ota, K. Yamada, T.G. Henares, K. Suzuki, D. Citterio, High-resolution microfluidic paper-based analytical devices for sub-microliter sample analysis, Micromachines 7 (5) (2016).
[18] Y.-J. Juang, P.-S. Chen, Y. Wang, Rapid fabrication of microfluidic paper-based analytical devices by microembossing, Sens. Actuators, B 283 (2019) 87–92.
[19] M.M. Thuo, R.V. Martinez, W.-J. Lan, X. Liu, J. Barber, M.B.J. Atkinson, D. Bandarage, J.-F. Bloch, G.M. Whitesides, Fabrication of low-cost paper-based microfluidic devices by embossing or cut-and-stack methods, Chem. Mater. 26 (14) (2014) 4230–4237.
[20] H. Kwangjoon, K. Kwang-Sun, K. Jaehwan, Au-pattern fabrication on a cellulose film using a polyurethane acrylate mold, J. Micromech. Microeng. 19 (3) (2009) 035010.
[21] J. Kim, S.-H. Bae, H.-G. Lim, Micro transfer printing on cellulose electro-active paper, Smart Mater. Struct. 15 (3) (2006) 889–892.
[22] A. Wolfberger, A. Petritz, A. Fian, J. Herka, V. Schmidt, B. Stadlober, R. Kargl, S. Spirk, T. Griesser, Photolithographic patterning of cellulose: a versatile dual-tone photoresist for advanced applications, Cellulose 22 (1) (2015) 717–727.
[23] E. Fu, C. Downs, Progress in the development and integration of fluid flow control tools in paper microfluidics, Lab Chip 17 (4) (2017) 614–628.
[24] C. Rivet, H. Lee, A. Hirsch, S. Hamilton, H. Lu, Microfluidics for medical diagnostics and biosensors, Chem. Eng. Sci. 66 (7) (2011) 1490–1507.
[25] M. Bialkower, C.A. Manderson, H. McLiesh, R.F. Tabor, G. Garnier, Paper diagnostic for direct measurement of fibrinogen concentration in whole blood, ACS Sens 5 (11) (2020) 3627–3638.
[26] M.J. Hertaeg, H. McLiesh, R.F. Tabor, G. Garnier, A rapid paper-based blood typing method from droplet wicking, Analyst (2021), https://doi.org/10.1039/D0AN01896A. In press.
[27] M.J. Hertaeg, R.F. Tabor, G. Garnier, Effect of protein adsorption on the radial wicking of blood droplets in paper, J. Colloid Interface Sci. 528 (2018) 116–123.
[28] D.L. Giokas, G.Z. Tsogas, A.G. Vlessidis, Programming fluid transport in paper-based microfluidic devices using razor-crafted open channels, Anal. Chem. 86 (13) (2014) 6202–6207.
[29] P. Raj, A. Mayahi, P. Lahtinen, S. Varanasi, G. Garnier, D. Martin, W. Batchelor, Gel point as a measure of cellulose nanofibre quality and feedstock development with mechanical energy, Cellulose 23 (5) (2016) 3051–3064.
[30] S. Varanasi, R. He, W. Batchelor, Estimation of cellulose nanofibre aspect ratio from measurements of fibre suspension gel point, Cellulose 20 (4) (2013) 1885–1896.
[31] K. Shanmugam, S. Varanasi, G. Garnier, W. Batchelor, Rapid preparation of smooth nanocellulose films using spray coating, Cellulose 24 (7) (2017) 2669–2676.
[32] K. Shanmugam, H. Doosthosseini, S. Varanasi, G. Garnier, W. Batchelor, Flexible spray coating process for smooth nanocellulose film production, Cellulose 25 (3) (2018) 1725–1741.
[33] M.J. Hertaeg, R.F. Tabor, J.D. Berry, G. Garnier, Dynamics of stain growth from sessile droplets on paper, J. Colloid Interface Sci. 541 (2019) 312–321.
[34] H. Gong, B.P. Bickham, A.T. Woolley, G.P. Nordin, Custom 3D printer and resin for 18 $\mu m \times 20$ μm microfluidic flow channels, Lab Chip 17 (17) (2017) 2899–2909.
[35] K. Shanmugam, H. Nadeem, C. Browne, G. Garnier, W. Batchelor, Engineering surface roughness of nanocellulose film via spraying to produce smooth substrates, Colloids Surf., A: Physicochem. Eng. Aspects 589 (2020).
[36] B. Wu, A. Kumar, S. Pamarthy, High aspect ratio silicon etch: A review, J. Appl. Phys. 108 (5) (2010) 051101.
[37] C. Kuo-Shen, A.A. Ayon, Z. Xin, S.M. Spearing, Effect of process parameters on the surface morphology and mechanical performance of silicon structures after deep reactive ion etching (DRIE), J. Microelectromech. Syst. 11 (3) (2002) 264–275.
[38] H. Becker, U. Heim, Hot embossing as a method for the fabrication of polymer high aspect ratio structures, Sens. Actuators, A 83 (1) (2000) 130–135.
[39] D.M. Cate, J.A. Adkins, J. Mettakoonpitak, C.S. Henry, Recent developments in paper-based microfluidic devices, Anal. Chem. 87 (1) (2015) 19–41.
[40] D. Yang, M. Krasowska, C. Priest, M.N. Popescu, J. Ralston, Dynamics of capillary-driven flow in open microchannels, J. Phys. Chem. C 115 (38) (2011) 18761–18769.
[41] C.K. Camplisson, K.M. Schilling, W.L. Pedrotti, H.A. Stone, A.W. Martinez, Two-ply channels for faster wicking in paper-based microfluidic devices, Lab Chip 15 (23) (2015) 4461–4466.
[42] A.W. Martinez, S.T. Phillips, M.J. Butte, G.M. Whitesides, Patterned paper as a platform for inexpensive, low-volume, portable bioassays, Angew. Chem. Int. Ed. 46 (8) (2007) 1318–1320.